IEEE Robotics and Automation Letters (RA-L) paper, presented at ICRA 2024, Yokohama, Japan. Cite as RA-L paper.

# AirTwins: Modular Bi-copters Capable of Splitting from Their Combined Quadcopter in Midair

Song Li[1], Fangyuan Liu[1], Yuzhe Gao, Jinwu Xiang, Zhan Tu*, and Daochun Li*

***Abstract*—Micro tandem bi-copters are capable of passing through narrow gaps owing to their particular slender shape. However, the introduction of the tilting servo motors leads to a non-minimum phase roll dynamics, which affects their flight stability when exploring environments with unpredictable disturbances. In this paper, we propose and design a re-configurable aerial platform consisting of two modular bi-copters with an undocking mechanism. In combined configuration, a crossover docking approach is employed to compensate for the poor stability in their servo-controlled attitude of each bi-copter. In bicopter configuration, the minimum size (equal to ideal passable gap's width) of the system was reduced by 58% through mid-air separation. In detail, to compare the attitude response of the two configurations, a dynamic model considering servo response and non-minimum phase is established and simulated, and flying poking experiments were also conducted on them respectively. On the other hand, the performance of single bi-copter including trajectory tracking and passing through narrow gaps was demonstrated through flight tests. Finally, the feasibility of the undocking mechanism was verified by mid-air separation experiments. The proposed system is promising to be applied in scenarios containing both complex perturbations and confined spaces, while also having the potential to improve exploration efficiency through collaborative work.**

***Index Terms*—Micro aerial robot, tilt-rotor bi-copter, modular design, mid-air separation, undocking mechanism design.**

## I. Introduction

To date, multi-rotor copters have become increasingly important in civil applications such as search-and-rescue missions. As a relatively mature micro air vehicle, they have good maneuverability and can help to effectively explore the environment [1]–[3]. An entire exploration mission often consists of two parts: one is approaching the target area, which usually requires the ability to withstand unpredictable external disturbances; The other is exploring the confined space of the target area, which requires a high level of access capability, such as crossing narrow gaps [4]–[6].

Taking the necessity for crossing confined spaces into consideration, tilt-rotor bi-copter (as shown in Fig. 1(a)) is worth mentioning because it has only two tiltable rotors arranged in tandem configuration like [7] and is inherently adaptable to tight spaces due to its slender shape (its width $d_W$ in the horizontal plane is much smaller than its length $d_L$ as shown in Fig. 1(b)). To date, a considerable amount of studies on the design, manufacture, and control of the bi-copters have been proposed [8]–[14]. Nevertheless, there are still two main issues that need conquering to further improve their application in complex environmental exploration. For one thing, the large size in width of the currently state-of-art bi-copters (rotor-base $>$ 20 cm) does not take advantage of their natural high access capability in profile. For another thing, the typical tandem layout of bi-copters tends to bring a practical control problem affecting the flight performance of tilt-rotor bi-copters, especially the micro bi-copters, in situations with unpredictable disturbances, such as lateral disturbances. The control problem includes the delay of the servo motor's response [15], and the non-minimized phase problem caused by the inner servo control torque [7], [16].

To confront the drawbacks of a single machine, multi-drone collaborative working has been a topic in recent years [17]–[25]. The concepts and feasibility of the collaborative work between a distributed flight array are first proposed and justified in [17]. In [19]–[21], the authors demonstrate a multi-linked and transformable aerial robot, which can accomplish versatile tasks including grasping different types of objects and

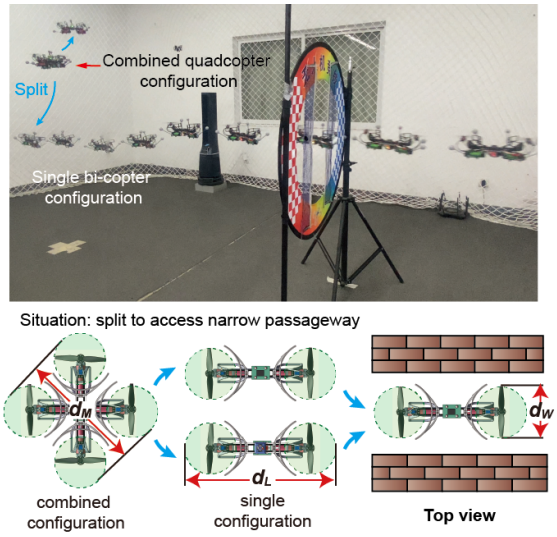


Fig. 1. Illustration of AirTwins flight modes and advantages in a mission situation: splitting to access a narrow passageway. Video is available at https://youtu.be/hskD3m1Ym_I

Manuscript received April, 5, 2023; revised June, 24, 2023; accepted July, 21, 2023. This paper was recommended for publication by Editor M. Ani Hsieh upon evaluation of the Associate editor and Reviewers' comments. This research received no specific grant from any funding agency in the public, commercial, or not-for-profit sectors.

[1] These authors contributed equally to this work.

* Corresponding Author: Zhan Tu and Daochun Li.

The authors are with the School of Aeronautic Science and Engineering, Beihang University, Beijing 100191, China. Jinwu Xiang is also with Tianmushan Laboratory, Xixi Octagon City, Yuhang District, Hangzhou 310023, China. Zhan Tu is also with the Institute of Unmanned System, Beihang University, Beijing 100191, China. (Email: zhantu@buaa.edu.cn, lidc@buaa.edu.cn)

Digital Object Identifier (DOI): see top of this page

IEEE Robotics and Automation Letters (RA-L) paper, presented at ICRA 2024, Yokohama, Japan. Cite as RA-L paper.

**IEEE Robotics and Automation Letters (RA-L) paper, presented at ICRA 2024, Yokohama, Japan. Cite as RA-L paper.**

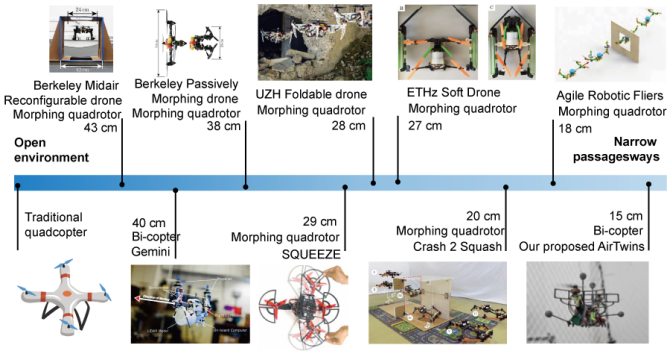


Fig. 2. Comparison of the capacity of drones to access narrow passageways reported in literature [4]–[7], [26]–[28].

passing through horizontal and small openings. In addition to the functional bonuses, multi-drone combinations are also used to improve the aerodynamic characteristics of the individual ones. For example, in [22], [23], the researchers design a meta-aircraft composed of two or more tilt-rotor aircraft, and the proposed meta-aircraft is proven to improve the aerodynamic efficiency by increasing the aspect ratio (wing span divided by mean chord) compared to a single one. Besides, the collaborative working of the drones also means that unexpected branching tasks can be dealt with in time during the mission [24], [25].

In this paper, we propose a re-configurable platform, AirTwins, which has two flight modes including a combined quadcopter mode and a splitting bi-copter mode (validated in Fig. 1). Compared with traditional bi-copters [7], our proposed platform conquers the minimum-phase dynamics caused by servo motors through combination of two modular bi-copters properly into a quadcopter configuration. While compared with other aerial re-configurable systems [25], [29]–[32], AirTwins can split into two modular bi-copters through the docking mechanism in the midair, keeping the passability of miniature bi-copter configuration. In this case, each of our proposed modular bi-copters is able to pass through a 15 cm gap, which is relatively small compared with other counterparts recorded in literature [4]–[7], [26]–[28](shown in Fig. 2). Thus, our proposed system is promising to meet with rescue or exploration missions which contain both open environment with disturbance and confined spaces with narrow gaps.

The rest of the article is organized as follows. Section II introduces the system design and implementation of the proposed platform. Section III presents the modeling procedure, control simulation, and the stability comparison analysis between the two flight modes of AirTwins. Section IV conducts the flight test and validates AirTwins advantages including stable flight and narrow gap passability. Section V summarizes the results and describes the future work.

## II. System Design

In this section, we first present the overall design configuration of the proposed bi-copter and assembled quadcopter, including its dimensions, weight, and individual components. Next, to achieve a tight connection and automatic separation of the combined quadcopter, a 6-DoF (in terms of number of

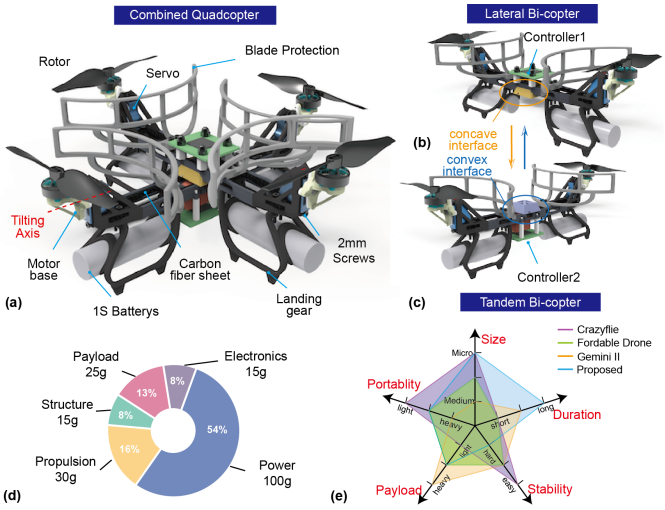


Fig. 3. Overview and main components of the proposed modular tilt-rotor bi-copter. (a) Rendered view of the combined quadcopter combined by two modular bi-copters in (b) and (c). (b) One of the modular bi-copter controlled in lateral configuration. (c) One of the modular bi-copter controlled in tandem configuration.(d) Comparison diagram between the proposed micro bi-copter with other micro air vehicles: core-less motor quadcopter Crazyflie [33], UZH foldable drone [26] and unconventional bi-copter Gemini II [8]. The size is defined as the minimum dimension in horizontal plane considering the rotor disk, which determines the width of the narrow gaps it can pass through.

constrained motion) docking mechanism driven by a single servo is developed. Finally, we further illustrate how the proposed bi-copter can achieve long flight endurance in such a small size.

### A. Overall Layout

To overcome the delayed servo response [15] and the non-minimum phase problem in the roll direction of a single bi-copter [7], [8], the combined quadrotor is constructed by two independent bi-copters with a '+' configuration rather than an 'H' configuration. As shown in Fig. 3(a), the two bi-copters are crossed and docked in the middle of their fuselage with a docking mechanism. As a consequence, the two bi-copters can be categorized into a lateral bi-copter (Fig. 3(b)) and a tandem bi-copter (Fig. 3(c)) according to their placement in the combined quadcopter. The difference between these two configurations lies in the implementation of two kinds of body coordinate frame, which will be illustrated in section III.

Here we define the minimum size of a copter as the minimum width of the narrow gaps it can theoretically pass through in the horizontal plane. The minimum size of the single bi-copter and combined quadcopter are depicted in Fig. 1(b) as $d_M$ and $d_W$ respectively. In the combined quadcopter configuration, this value is 24.2cm considering the propeller tip length. In contrast, the single bi-copter has a slender configuration, in which its width $d_W$ is 10.1cm and tip length $d_L$ 29.5cm. Compared to the combined quadrotor, its minimum dimensions are reduced by about $1 - d_W/d_M = 58\%$.

The total weight of the proposed bi-copter is 185 grams. The components and hardware of the two bi-copters are exactly the same (except for the docking mechanism), which can be

**IEEE Robotics and Automation Letters (RA-L) paper, presented at ICRA 2024, Yokohama, Japan. Cite as RA-L paper.**

TABLE I
TYPES AND WEIGHTS OF EACH COMPONENTS

| Component | Num | Type | Weight |
|---|---|---|---|
| BLDC Motor | 2 | HGLRC 1303.5 | 6.5 |
| Tilt Servo | 2 | KST X06 | 6.0 |
| Battery | 2 | NCR18650GA | 50 |
| Flight Controller | 1 | MATEKSYS H743-MINI | 7 |
| ESC | 2 | EMAX 6A | 3.2 |
| Undocking Servo† | 1 | BlueArrow 3018MG | 3.4 |

† this servo only exists in the tandem configuration bicopter.

broken down into categories as shown in Fig. 3(d). Each bi-copter mainly consists of five parts including the propulsion system (two tiltable rotor modules), the power supply, onboard electronics, the payload and the 3D printed structure. The weights and types of each component are listed in table I.

The main advantage of the proposed micro bi-copter to the existing copters lies in its ability to achieve longer flight time and smaller size at the same time, as shown in Fig. 3(e). The width of the proposed bi-copter ($d_W = 10.1$cm) is very close to the width of a DC core-less quadcopter (such as Crazyflie 2.1 [33], $d_M = 11$cm), but it has a longer flight time of 25 minutes.

On the other hand, for the combined configuration, it has more control degrees due to the introducing of four additional servo motors. Thus, compared with traditional quadcopter, it is also potential to achieve some other maneuvers like the tilt-rotor drones [34].

### B. Undocking Mechanism

The main purpose of the docking mechanism is to ensure the tight connection between the two bi-copters, based on which the rigid body assumption can be promised and used in section III. At the same time, the docking mechanism is also designed to be able to unlock by a servo motor. In this case, when the combined quadcopter encounters a confined environment, it is capable of decomposing into two separate bi-copters to perform the required tasks separately.

As shown in Fig. 4(A), the compact docking mechanism can be divided into two wedge-shaped interfaces, one of which is concave and the other is convex. Their surfaces are designed to have a slope, which is to ensure that the docking mechanism can transmit the six-degree forces and moments between the two vehicles when combined. In addition, a linear spring is implemented between the two docking interfaces, which can accelerate the separation process and also provide an internal bracing force when locked.

As shown in Fig. 4(B), the locking mechanism is composed of a coulisse wheel, a digital servo which is used to drive the wheel, and four 1mm diameter stainless steel locking rods with one end folded into a Z shape and inserted in the slide of the wheel. When it is needed to unlock the docking mechanism, the wheel will be driven clockwise, and the locking rod will slide into the slot and withdraw from the holes through the two connecting surfaces. When needed to be locked, the servo will be driven in the opposite direction.

The kinematic relationship of the rotating angle of the servo motor and the displacement of the four locking rods can be

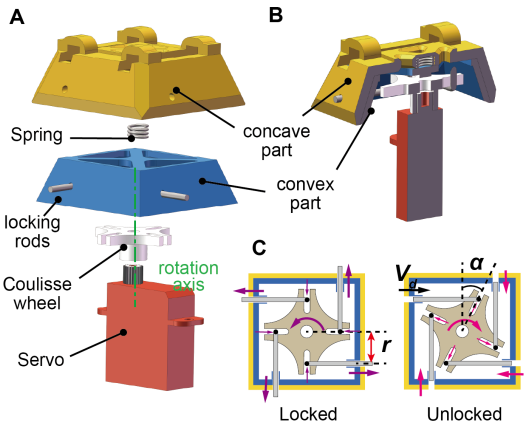


Fig. 4. Illustration of docking and locking mechanism. (A) Cross-sectional view and main components of designed docking mechanism in the locked state. (B) Top view of the locking mechanism in the locked and unlocked state and the kinematic relationship of each part.

formulated into

$$d = r\tan(\alpha) \tag{1}$$

$$V_d = r\frac{\dot{\alpha}}{\cos^2(\alpha)} \tag{2}$$

where $d$ is the displacement of the locking rod, $\alpha$ is the angle of the servo deviated from the center position. $r$ is the constant distance (5mm) from the rotation center to the moving rod.

According to equation (1), the servo needs to rotate at least 17 degrees to unlock the mechanism. At an average servo rotation speed of 923 degrees per second (from BlueArrow database), this process takes about 18ms, which is fast enough to reduce the separation process on the control of the two bi-copters.

### C. Propulsion Selection for Long-endurance Flight

It is worth noting that, within the constraints of a narrow space of the same size, the bi-copter configuration has a naturally efficient flight ability compared with the same size ($d_M = d_W$) of quadcopter [7]. According to [35], the hovering power requirement $P_h$ of a multicopter is given by

$$P_h = \frac{(mg)^{3/2}}{\eta_p\sqrt{2\rho\pi N_r R_p}} \tag{3}$$

where $\eta_p$ is the propeller efficiency, $N_r$ is the number of rotors, $R_p$ is the radius of the propeller, $m$ is the takeoff weight, $g$ is gravity, $\rho$ is air density.

Given a fixed width of the narrow gap, the bi-copter configuration has 2 times of the radius $R_p$ and half of the rotor number $N_r$, compared with the quadcopter. This will result in a 30% reduction of the power consumption at hover and thus increase the flight time. Although the additional servo motors will bring extra weight, this part of weight in our bicopter is only 6% of the takeoff weight and will not eliminate the reduction in power consumption that comes from the increased efficiency of the propeller

However, with the reduced size, sufficient thrust as well as efficiency are challenges for rotoring wings [36], [37]. In this case, in order to trade-off between flight efficiency and

**IEEE Robotics and Automation Letters (RA-L) paper, presented at ICRA 2024, Yokohama, Japan. Cite as RA-L paper.**

TABLE II
PARAMETERS OF BLUSHLESS MOTORS AND PROPELLERS USED IN EXPERIMENT

| Motor | 1 | 2 | 3 |
|---|---|---|---|
| Stator diameter (mm) | 11 | 12 | 13 |
| Stator height (mm) | 3 | 4 | 3.5 |
| KV value | 8000 | 5000 | 4500 |
| **Propeller** | **1** | **2** | **3** |
| Diameter (mm) | 65 | 75.8 | 101.1 |
| Pitch (inch) | 1.3 | 1.5 | 2.4 |
| Blade number | 2 | 2 | 2 |

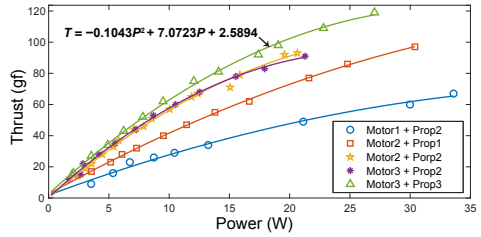


Fig. 5. Experiment results of the input power versus the thrust by different motor and propeller combinations listed on table II. The tested voltage is 8V.

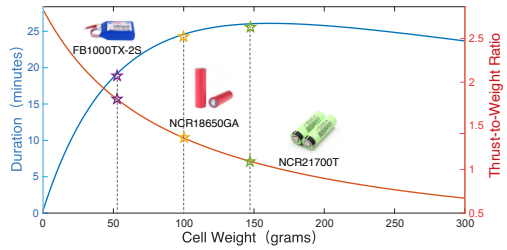


Fig. 6. Effect of battery mass on hovering flight time and the thrust-to-weight ratio of the proposed bi-copter.

passability of the proposed bicopter, we compared different propellers from 65mm to 101mm accompanied by three types of micro brushless motors with different stator diameters and heights as listed in table II. A series of thrust experiments were conducted, and the power requirement and thrust results were measured as shown in Fig. 5. The combination of motor 3 and propeller 3 could achieve the highest efficiency of 0.0549N/W and a maximum thrust of 1.18N.

With the poly-fitted equation shown in Fig. 5, a theoretical ideal flight endurance could be estimated as

$$T_d = \frac{\rho_c M_{cell}}{2f^{-1}\left(\frac{M_{cell}+M_{fix}}{2}\right)} \tag{4}$$

where $T_d$ is the flight endurance. $\rho_c$ is the average energy density of selected batteries as 0.167Wh/grams. $M_{fix}$ is the fixed mass of 85grams. $M_{cell}$ is the mass of selected battery. $f^{-1}()$ is the reversed function of Thrust-to-Power equation in Fig. 5.

As shown in Fig. 6, the relationship between flight time and battery weight is calculated and three types of lithium-ion batteries are compared. With a battery weight of over 100 grams, there is no significant tendency for the flight time to increase, while the thrust-to-weight ratio is too low to produce sufficient control torque. Therefore, the NCR18650GA battery with 3000mAh capacity is finally integrated.

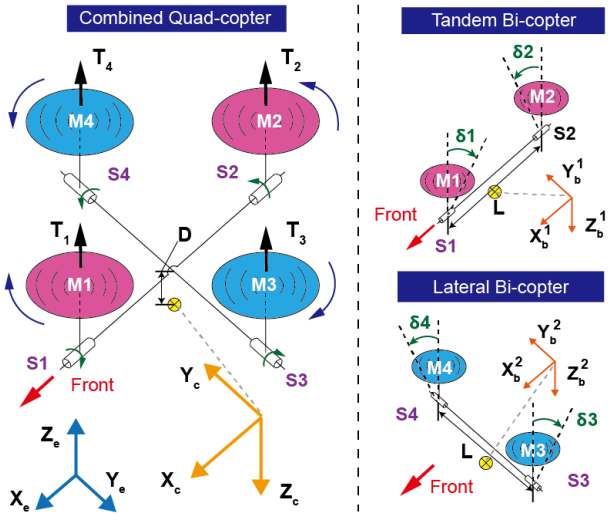


Fig. 7. Coordinates definition and control degrees of the two bi-copters and combined quadcopter. $D$ is the distance between the tilting axis and mass center as 38mm, $L$ is the distance between two rotors' axis as 194mm. The yellow dot represents the center of gravity of each configuration. The purple arrow denotes the positive direction of motor rotation, and the green arrow denotes the servo motor's positive direction.

## III. MODELLING AND STABILITY COMPARISON

In order to guarantee the independent flight capability after disassembling, the two bi-copters in the combined quadcopter are implemented with two separate flight controllers as shown in Fig. 3(b)(c). Therefore, it is crucial to ensure that these two controllers collaborate effectively when flying together.

As shown in Fig. 7, the two kinds of bi-copters are docked in the middle of their fuselage by a '+' shaped crossover, so that the directions controlled by their servo motors (roll for tandem, pitch for lateral) can be compensated by each other. The tandem bi-copter uses differential motor speed to move forward similar to [7], while the lateral bi-copter uses servo deflection to generate forward forces similar to [13].

The modelling process and the effectiveness of this configuration in addressing the non-minimum phase problems are illustrated in the following.

### A. Coordinate frames

In order to express the relationship between the control forces and moments of the two bi-copters during combination, three coordinate frames are introduced:

*1) Earth coordinate frame $X_eY_eZ_e$ :* also called inertial frame.The aircraft attitude can be represented by three Euler angles in this frame, as pitch $\theta$, roll $\phi$, and yaw $\psi$.

*2) Bi-copter coordinate frame $X_b^iY_b^iZ_b^i$ :* $i$ = 1 for tandem bi-copter, $i$ = 2 for lateral bi-copter. The origin of these frames are fixed on the mass center of each bi-copter. The $x_b^1$-axis is parallel to the line connecting the two motors, while the $x_b^2$-axis is perpendicular to this direction. $z_b^i$ pointing down to the ground.

*3) Combined quadcopter coordinate frame $X_cY_cZ_c$ :* the origin is attached to the mass center of the combined quadrotor, which is considered as a rigid body, the x-axis coincides with the $x_b^1$-axis of the tandem bi-copter. $z_c$ pointing

**IEEE Robotics and Automation Letters (RA-L) paper, presented at ICRA 2024, Yokohama, Japan. Cite as RA-L paper.**

**IEEE Robotics and Automation Letters (RA-L) paper, presented at ICRA 2024, Yokohama, Japan. Cite as RA-L paper.**

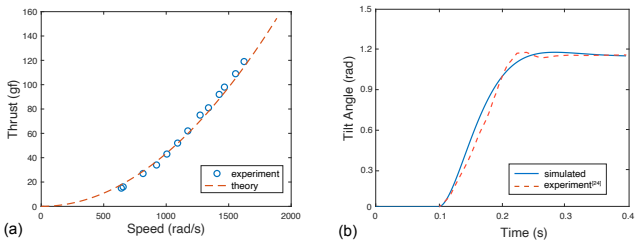


Fig. 8. (a) Comparison between the blade element theory and experiment results of the motor speed versus the thrust force. The propeller speed was measured using a non-contact laser tachometer.(b) Step response comparison between established servo delay model and the experimental results in figure 3(b) of reference [15].

down to the ground. The angular velocity of in this frame is defined by $\boldsymbol{\omega} = [p, q, r]^T$

Thus, in the combined flight mode, the Euler angles and angular velocities of each individual bi-copter are consistent with each other and with the combined body, i.e.,

$$[\theta, \phi, \psi] = [\theta_i, \phi_i, \psi_i], \quad \omega = \omega_i, \quad i = 1, 2 \tag{5}$$

### B. Control Forces and Moments

After receiving the attitude feedback from the combined quadcopter, each controller sent the control signal to its own two motors and two servo motors based on their own control strategy. The control torque $\boldsymbol{\tau}_c^i$ generated by the two configuration of bi-copters are written into

$$\boldsymbol{\tau}_c^i = \sum_{j=2i-1}^{2i} \mathbf{R}(\beta_i)\mathbf{T}_j \times \mathbf{l}_j + \sum_{j=2i-1}^{2i} \mathbf{R}(\beta_i)\mathbf{M}_j, \quad i = 1, 2 \tag{6}$$

where $j$ donates the $j$th rotor in Fig. 7. $\mathbf{R}(\beta_i) \in SO(3)$ is the rotation matrix around the z-axis by angle $\beta_i$ ($\beta_1 = 0$, $\beta_2 = 90$). $\mathbf{l}_j$ is the location of the $j$th motor in the body frame, for example, $\mathbf{l}_1 = [L/2, 0, -D]^T$. $\mathbf{T}_j$ and $\mathbf{M}_j$ are the thrust force vector and torque respectively. They are calculated based on the equations (6.17)-(6.18) of reference [38], with tilt angle $\delta_j$, and can be written in the body frame $X_cY_cZ_c$ as

$$\mathbf{T}_j = \mathbf{R}(\delta_j)\mathbf{e}_3 C_T \rho N_j^2 R_p^4 \tag{7}$$

$$\mathbf{M}_j = (-1)^{j-1}\mathbf{R}(\delta_j)\mathbf{e}_3 C_M \rho N_j^2 R_p^5 \tag{8}$$

where $\mathbf{R}(\delta_j) \in SO(3)$ is the rotation matrix w.r.t the tilting angle of $j$th rotor. $\mathbf{e}_3 = [0, 0, 1]^T$. $N_j$ is the $j$th motor speed. $R_p$ is the radius of the propeller. $C_T$ and $C_M$ are the dimensionless thrust and torque coefficients respectively, which can be modeled and calculated by the blade element theory [39] as

$$\begin{aligned} C_T &= 0.25\pi^3 \lambda \zeta^2 B_p K_0 \frac{\epsilon \arctan(H_p/\pi D_p) - \alpha_0}{\pi A + K_0} \\ C_M &= \frac{1}{8A}\pi^2 C_d \zeta^2 \lambda {B_p}^2 \end{aligned} \tag{9}$$

where the blade number $B_p$ is 2, the aspect ratio $A$ is 7, the pitch $H_p$ is 61mm, the area correction factor $\lambda$ is 0.75, the downwash factor $\epsilon$ is 0.85, the average blade speed factor $\zeta$ is 0.5, $K_0$ is a constant as 6.11 and drag coefficient $C_d$ is empirically estimated as 0.0671 to fit the experimental results. With these constants, the $C_T$ and $C_M$ are calculated as 0.129 and 0.0067 respectively. The servo model is established based on the first-order motor model with a PD feedback controller. The comparison results of the established model and experimental results are shown in Fig. 8.

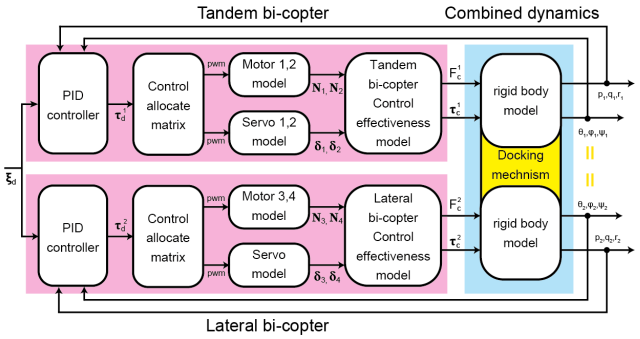


Fig. 9. Attitude control block diagram of each bi-copter and the control structure of the combined quadcopter. The purple backgrounds represent the two independent bi-copter attitude controllers. The blue background represents the combined dynamic model of the quad-copter.

### C. Attitude Control

The attitude controller is a cascaded PID controller as shown in Fig. 9, which consists of an outer loop proportional angular control and an inner angular rate loop. The outer loop is used to track the desired attitude $\xi_d$, and output the desired angular rate $\omega_d$ to the inner loop which can be written as:

$$\omega_e = \omega_d - \omega \tag{10}$$

$$\tau_d^i = K_p^i \omega_e + K_i^i \int \omega_e + K_d^i \dot{\omega}_e, \quad i = 1, 2 \tag{11}$$

where $\omega_e$ and $\omega_d$ are the error and desired angular velocity. $K_p^i$, $K_i^i$, and $K_d^i$ are the PID parameters of the inner loop.

### D. Dynamic Modelling

The overall dynamics including attitude controller of the combined quadrotor are shown in Fig. 9, where the control effectiveness models for the two bi-copter configurations have been given in equations (6)-(8). Here, the combined attitude dynamics equation of the bi-copters is established by combining of two rigid body dynamics equation of the bicopters, which is written in the frame $X_cY_cZ_c$ as

$$\sum_{i=1}^{2} \mathbf{I}_b^i \dot{\boldsymbol{\omega}} + \boldsymbol{\omega} \times \sum_{i=1}^{2} \mathbf{I}_b^i \boldsymbol{\omega} = \sum_{i=1}^{2} \boldsymbol{\tau}_c^i + \sum_{j=1}^{4} \boldsymbol{\tau}_r^j \tag{12}$$

where $I_b^i$ represents the inertia matrix of the $i$th bi-copter in the frame $X_b^iY_b^iZ_b^i$, $\boldsymbol{\tau}_c^i$ is the control torque given by equation (6). $\boldsymbol{\tau}_r^j$ is the reaction torque caused by $j$th tilting servo with a tilt angle $\delta_j$. According to [16] , it can be formulated by

$$\boldsymbol{\tau}_r^j = I_m \mathbf{R}(\beta_i)\mathbf{e}_1 \ddot{\delta}_j \tag{13}$$

where $I_m$ is the inertia of a set of motor and propeller around the tilting axis. $\mathbf{e}_1 = [1, 0, 0]^T$. The sign of these reaction torque dependent on the sign of $\ddot{\delta}_j$, whose positive directions are depicted by the arrows shown in Fig. 7.

**IEEE Robotics and Automation Letters (RA-L) paper, presented at ICRA 2024, Yokohama, Japan. Cite as RA-L paper.**

TABLE III
SIMULATION PARAMETER

| Parameter | Value | Unit |
|---|---|---|
| ${I_{ix}}^b$ Inertia matrix components | $1.49 \times 10^{-4}$ | $\mathrm{kg.m}^2$ |
| ${I_{iy}}^b$ Inertia matrix components | $5.01 \times 10^{-4}$ | $\mathrm{kg.m}^2$ |
| ${I_{iz}}^b$ Inertia matrix components | $3.65 \times 10^{-4}$ | $\mathrm{kg.m}^2$ |
| $I_m$ tilt-rotor inertia of moment | $1.9 \times 10^{-6}$ | $\mathrm{kg.m}^2$ |

the inertia matrix are calculated from the 3D CAD model in Fig.3.

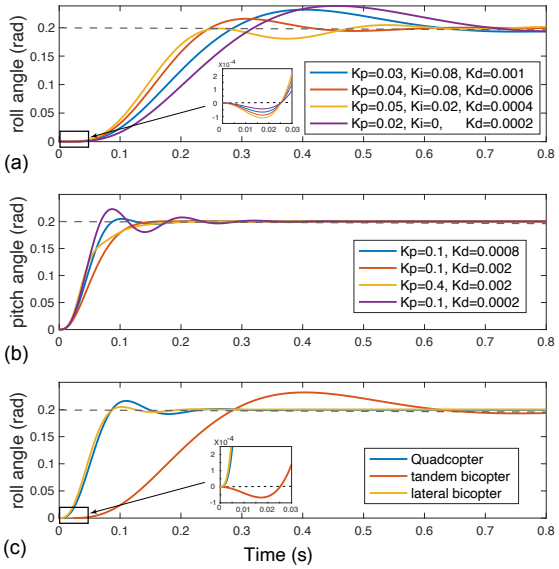


Fig. 10. (a) The simulated dynamic response of a step desired roll angle with different PID parameters. As can be seen from the zoomed-in box of the initial stage, the roll channel is a non-minimum phase system due to the inner servo drive torque. (b) The simulated dynamic response of a step desired pitch angle with different PD parameters. (c) Comparison of the dynamic response of the same PID parameter in (a)(b) between bi-copter and combined quadcopter.

### *E. Simulation and Analysis*

The system model of a single bi-copter and the combined configuration model are implemented in MATLAB. With the geometry parameters listed in table.III, the equilibrium normalized throttle input value is calculated as 0.577 (range from 0-1). The open-loop transfer function for the roll direction of a tandem bi-copter is solved through the linearization toolbox in MATLAB as:

$$G(z) = \frac{-0.00267(z-1.001)(z-0.9987)(z^2-2z+0.9995)}{z(z-1)^5} \tag{14}$$

According to the transfer function, the roll channel controlled by tilt servo motor has two zeros out of the unit circle (z=1.001, z=1.024) in the z plane, which presents the roll channel as a non-minimum phase system.

In order to compare the dynamic response performance of combined configuration with a single bi-copter, a step desired roll signal with an amplitude of 0.2 rad is input into their dynamic models respectively. Different PID parameters are adopted to generate better response performance. According to results shown in Fig. 10(a), the $K_p = 0.04, K_i = 0.08, K_d = 0.0006$ pair could achieve a better response in rolling direction. Due to the reaction torque caused by the tilting motion of the servo, the roll angle of the tandem bi-copter will dip down at the beginning of the response, which is also presented and explained in [15], [16]. It is worth noting that the counter roll is more obvious with the increase of parameter $K_p$ and the moment of inertia of the tilt part. In contrast, as shown in Fig. 10(b), the response time is shorter in the pitch direction, and the $K_p = 0.1, K_d = 0.0008$ pair can achieve a better response. When combining the tandem bi-copter and the lateral bi-copter with the same PID parameters used in Fig. 10(a)(b), the rolling response is more rapid and improved obviously as shown in Fig.10(c).

## IV. EXPERIMENTAL VALIDATION

### *A. Single bi-copter flight test*

The flight tests are mainly used to verify the actual flight performance of the proposed micro bi-copters and can be divided into trajectory tracking flight tests and narrow gap tests.

In the trajectory tracking test, the reference position is preset and generated offline and uploaded to the flight control board before flight. The sequence diagram of the bi-copter tracking the flight trajectory is shown in Fig. 11(a). A small GPS module (Beitian BN-880, 5.3g) is implemented to provide the 3D position information.

The horizontal plane uses proportional control to convert the position error to the target velocity. Then a velocity PID controller was used to convert the velocity error to the required acceleration, which is finally transformed to the required desired angle and sent to the attitude controller. The comparison between targeted position and velocity and real position and velocity are shown in Fig. 11(b). According to the results, the proposed micro bi-copter successfully followed the trajectory as shown in Fig. 11(c). A maximum velocity of 7m/s could be achieved in the test and the velocity errors are within 2m/s as shown in Fig. 11(d)(e).

In the test of traversing a narrow gap, a 15cm wide by 30cm high tunnel was cut out and placed in the middle of the motion capture field, which was used to provide the 3D positioning information. The time-series sequence of the bi-copter passing through the narrow gap is shown in Fig. 11(f). In the experiment, the tandem bi-copter first took off, then approached and aligned itself with the narrow gap it was going to traverse, and finally flew forward and through by rapidly changing attitude angle in the pitch channel, as shown in Fig. 11(g)(h). The small lateral flight error of the vehicle ensures that it passes quickly through the narrow space without collision.

### *B. Stability validation*

In order to verify the stability strength of the combined quadcopter compared with a single bi-copter, we conducted disturbance experiments by poking the combined quadcopter and bi-copter respectively at hovering. In the experiments, we manually poke the fuselage of the two aircraft with plastic sticks to create an angle inclination in the pitch attitude. During this process, both aircraft were hovering in the motion capture system, with expectations of the position controller held constant. The attitude results in a poking direction and their positions are shown in Fig. 12(a)(b). As can be seen from

**IEEE Robotics and Automation Letters (RA-L) paper, presented at ICRA 2024, Yokohama, Japan. Cite as RA-L paper.**

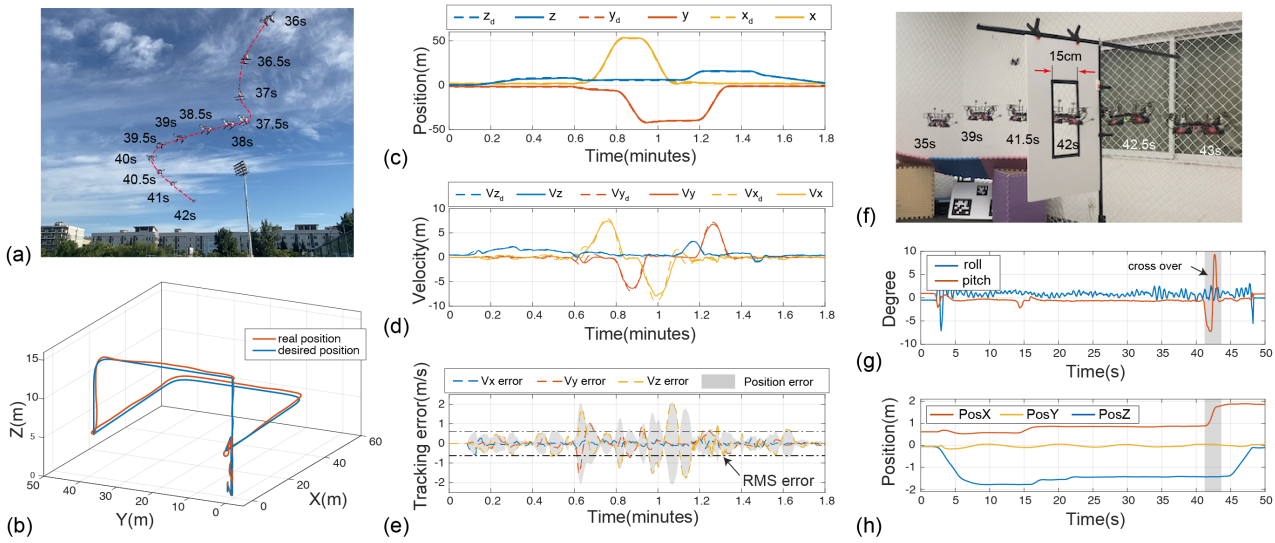


Fig. 11. (a) Compound photograph of the proposed micro bi-copter in tracking the rectangular trajectory from a random starting point and the opposite heading direction. (b) The trajectory tracking results of the proposed micro bi-copter in 3D view. (c)-(d) The time course of the 3D position, velocity, and tracking errors of the trajectory tracking flight. (f) Composite image of the process passing through a 15cm width narrow gap. (g)-(h) The flight attitude and 3D trajectory of the whole procedure from takeoff to landing.

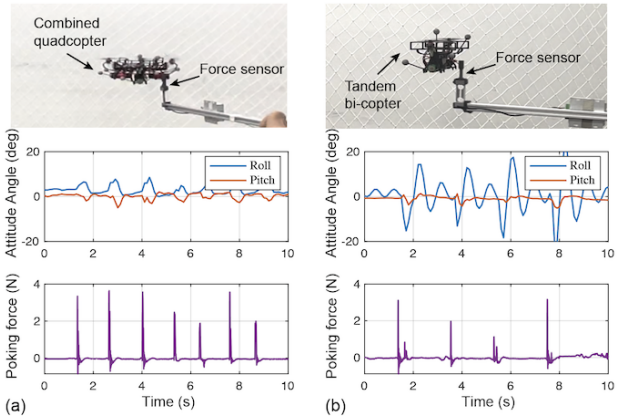


Fig. 12. Attitude response and poking force of the tandem bi-copter being excited by random poking in (a) combined configuration and (b) single bi-copter configuration respectively.

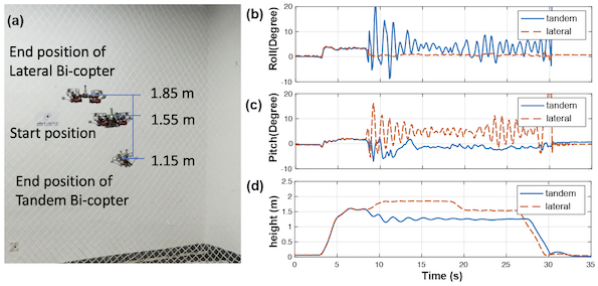


Fig. 13. Image that records the mid-air separation of the two modular bi-copters. (a) The height variance of each vehicles during decoupling process. And the flight data of (b) roll angle, (c) pitch angle and (d) height of the two modular bi-copters during splitting.

the figure, using the crossover docking approach in section III, the attitude angle of the combined quadrotor can quickly converge to a steady state after the perturbation. In contrast, the tandem bi-copter needs a longer time to recover due to the slow servo response in the roll direction and the non-minimum phase problem.

### C. Separating demonstration

In order to verify the capability of the proposed air separation of the bi-copters and the design of the undocking mechanism, a midair disassembly experiment was carried out. The experiment was divided into three stages: firstly, the two bi-copters were pre-assembled on the ground and took off in a quad-rotor mode; secondly, the separation mechanism was unlocked and the two bi-copters performed an aerial separation. Through following the predetermined trajectory, the height variation in separation could be minimized into 0.4m of the below bicopter. Finally, the two bi-copters performed an independent flight. The timing diagram of the whole separation experiment is shown in Fig. 13(a), and the flight test data of the two tested bi-copters including altitude and attitude angle are shown in Fig. 13(b)-(d).

## V. Conclusion and Future Work

In this paper, we propose a re-configurable platform called AirTwins which integrates both the stability advantage of quadcopter configuration and accessibility advantage of bi-copter configuration. The proposed system mainly consists of two modular tilt-rotor bi-copters and a mid-air undocking mechanism. And it is promising to meet with rescue or exploration missions containing both outdoor environment with unexpected disturbance and confined spaces, which are validated by the poking experiments and narrow gap traversing tests respectively. Besides, we established a systematic dynamic model of the proposed modular bi-copter. Compared to the existing bi-copter model, the proposed one considers both a specific servo motor model with actual response delay and the non-minimum phase problem. Such a specific model facilitates further exploration of bi-copter control algorithms in the future.

**IEEE Robotics and Automation Letters (RA-L) paper, presented at ICRA 2024, Yokohama, Japan. Cite as RA-L paper.**

The integrating AirTwins platform we proposed here tends to be extremely promising to carry out missions containing both complex outdoor flight situations and narrow indoor flight situations. Additionally, the docking mechanism also makes it possible that the drones respond to unexpected branching tasks during a mission in time. Hence, future work will be mainly based on the mission requirements under these circumstances and includes (1) Study on the aerodynamic interface of the two bi-copters to address the constrain of flight height during undocking process in the midair; (2) Docking strategy in the midair autonomously with electromagnet guidance; (3) Communication strategy between two bi-copters to achieve collaborative work after separation.

## REFERENCES


[1] D. Floreano and R. J. Wood, "Science, technology and the future of small autonomous drones," *nature*, vol. 521, no. 7553, pp. 460–466, 2015.

[2] M. Hassanalian and A. Abdelkefi, "Classifications, applications, and design challenges of drones: A review," *Progress in Aerospace Sciences*, vol. 91, pp. 99–131, 2017.

[3] M. Idrissi, M. Salami, and F. Annaz, "A review of quadrotor unmanned aerial vehicles: Applications, architectural design and control algorithms," *Journal of Intelligent & Robotic Systems*, vol. 104, no. 2, pp. 1–33, 2022.

[4] A. Fabris, E. Aucone, and S. Mintchev, "Crash 2 squash: An autonomous drone for the traversal of narrow passageways," *Advanced Intelligent Systems*, vol. 4, no. 11, p. 2200113, 2022.

[5] V. Riviere, A. Manecy, and S. Viollet, "Agile robotic fliers: A morphing-based approach," *Soft robotics*, vol. 5, no. 5, pp. 541–553, 2018.

[6] N. Bucki, J. Tang, and M. W. Mueller, "Design and control of a midair-reconfigurable quadcopter using unactuated hinges," *IEEE Transactions on Robotics*, 2022.

[7] Y. Qin, W. Xu, A. Lee, and F. Zhang, "Gemini: A compact yet efficient bi-copter uav for indoor applications," *IEEE Robotics and Automation Letters*, vol. 5, no. 2, pp. 3213–3220, 2020.

[8] Y. Qin, N. Chen, Y. Cai, W. Xu, and F. Zhang, "Gemini ii: Design, modeling, and control of a compact yet efficient servoless bi-copter," *IEEE/ASME Transactions on Mechatronics*, vol. 27, no. 6, pp. 4304–4315, 2022.

[9] M. M. de Almeida Neto, "Control strategies of a tilt-rotor uav for load transportation," 2014.

[10] L. Hrečko, J. Slačka, and M. Halás, "Bicopter stabilization based on imu sensors," in *2015 20th International Conference on Process Control (PC)*. IEEE, 2015, pp. 192–197.

[11] K. Kawasaki, Y. Motegi, M. Zhao, K. Okada, and M. Inaba, "Dual connected bi-copter with new wall trace locomotion feasibility that can fly at arbitrary tilt angle," in *2015 IEEE/RSJ International Conference on Intelligent Robots and Systems (IROS)*. IEEE, 2015, pp. 524–531.

[12] Ö. B. Albayrak, Y. Ersan, A. S. Bağbaşı, A. T. Başaranoğlu, and K. B. Arıkan, "Design of a robotic bicopter," in *2019 7th International Conference on Control, Mechatronics and Automation (ICCMA)*. IEEE, 2019, pp. 98–103.

[13] Q. Zhang, Z. Liu, J. Zhao, and S. Zhang, "Modeling and attitude control of bi-copter," in *2016 IEEE International Conference on Aircraft Utility Systems (AUS)*. IEEE, 2016, pp. 172–176.

[14] H. B. AKYILDIZ, İ. KACAR, and M. K. YALCIN, "Parameter optimization of a bi-copter type unmanned aerial vehicle to avoid propeller-induced vibrations during hovering," *Sakarya University Journal of Science*, vol. 24, no. 4, pp. 685–693, 2020.

[15] X. He and Y. Wang, "Design and trajectory tracking control of a new bi-copter uav," *IEEE Robotics and Automation Letters*, vol. 7, no. 4, pp. 9191–9198, 2022.

[16] Y. Li, Y. Qin, W. Xu, and F. Zhang, "Modeling, identification, and control of non-minimum phase dynamics of bi-copter uavs," in *2020 IEEE/ASME International Conference on Advanced Intelligent Mechatronics (AIM)*. IEEE, 2020, pp. 1249–1255.

[17] R. Oung, A. Ramezani, and R. D'Andrea, "Feasibility of a distributed flight array," in *Proceedings of the 48h IEEE Conference on Decision and Control (CDC) held jointly with 2009 28th Chinese Control Conference*. IEEE, 2009, pp. 3038–3044.

[18] R. Oung and R. D'Andrea, "The distributed flight array: Design, implementation, and analysis of a modular vertical take-off and landing vehicle," *The International Journal of Robotics Research*, vol. 33, no. 3, pp. 375–400, 2014.

[19] M. Zhao, K. Kawasaki, X. Chen, S. Noda, K. Okada, and M. Inaba, "Whole-body aerial manipulation by transformable multirotor with two-dimensional multilinks," in *2017 IEEE International Conference on Robotics and Automation (ICRA)*. IEEE, 2017, pp. 5175–5182.

[20] M. Zhao, F. Shi, T. Anzai, K. Chaudhary, X. Chen, K. Okada, and M. Inaba, "Flight motion of passing through small opening by dragon: Transformable multilinked aerial robot," in *2018 IEEE/RSJ International Conference on Intelligent Robots and Systems (IROS)*. IEEE, 2018, pp. 4735–4742.

[21] M. Zhao, T. Anzai, F. Shi, X. Chen, K. Okada, and M. Inaba, "Design, modeling, and control of an aerial robot dragon: A dual-rotor-embedded multilink robot with the ability of multi-degree-of-freedom aerial transformation," *IEEE Robotics and Automation Letters*, vol. 3, no. 2, pp. 1176–1183, 2018.

[22] S. J. Carlson and C. Papachristos, "The minihawk-vtol: Design, modeling, and experiments of a rapidly-prototyped tiltrotor uav," in *2021 International Conference on Unmanned Aircraft Systems (ICUAS)*. IEEE, 2021, pp. 777–786.

[23] S. J. Carlson, P. Arora, and C. Papachristos, "A multi-vtol modular aspect ratio reconfigurable aerial robot," in *2022 International Conference on Robotics and Automation (ICRA)*. IEEE, 2022, pp. 8–15.

[24] S. Bai, S. Tan, and P. Chirarattananon, "Splitflyer: A modular quadcoptor that disassembles into two flying robots," in *2020 IEEE/RSJ International Conference on Intelligent Robots and Systems (IROS)*. IEEE, 2020, pp. 1207–1214.

[25] S. Bai and P. Chirarattananon, "Splitflyer air: A modular quadcopter that disassembles into two bicopters mid-air," *IEEE/ASME Transactions on Mechatronics*, 2022.

[26] D. Falanga, K. Kleber, S. Mintchev, D. Floreano, and D. Scaramuzza, "The foldable drone: A morphing quadrotor that can squeeze and fly," *IEEE Robotics and Automation Letters*, vol. 4, no. 2, pp. 209–216, 2018.

[27] N. Bucki and M. W. Mueller, "Design and control of a passively morphing quadcopter," in *2019 International Conference on Robotics and Automation (ICRA)*. IEEE, 2019, pp. 9116–9122.

[28] A. Fabris, S. Kirchgeorg, and S. Mintchev, "A soft drone with multi-modal mobility for the exploration of confined spaces," in *2021 IEEE International Symposium on Safety, Security, and Rescue Robotics (SSRR)*. IEEE, 2021, pp. 48–54.

[29] Z. Wu, R. Zhao, M. Yu, Y. Zhao, W. Yang, W. Zhang, and F. Li, "Design, modeling and control of a composable and extensible drone with tilting rotors," in *2022 IEEE/RSJ International Conference on Intelligent Robots and Systems (IROS)*. IEEE, 2022, pp. 12 682–12 689.

[30] D. Saldana, P. M. Gupta, and V. Kumar, "Design and control of aerial modules for inflight self-disassembly," *IEEE Robotics and Automation Letters*, vol. 4, no. 4, pp. 3410–3417, 2019.

[31] D. Saldana, B. Gabrich, G. Li, M. Yim, and V. Kumar, "Modquad: The flying modular structure that self-assembles in midair," in *2018 IEEE International Conference on Robotics and Automation (ICRA)*. IEEE, 2018, pp. 691–698.

[32] K. P. Jain and M. W. Mueller, "Flying batteries: In-flight battery switching to increase multirotor flight time," in *2020 IEEE International Conference on Robotics and Automation (ICRA)*. IEEE, 2020, pp. 3510–3516.

[33] Crazyflie 2.1 — bitcraze. [Online]. Available: https://www.bitcraze.io/products/crazyflie-2-1/

[34] P. Zheng, X. Tan, B. B. Kocer, E. Yang, and M. Kovac, "Tiltdrone: A fully-actuated tilting quadrotor platform," *IEEE Robotics and Automation Letters*, vol. 5, no. 4, pp. 6845–6852, 2020.

[35] L. Bauersfeld and D. Scaramuzza, "Range, endurance, and optimal speed estimates for multicopters," *IEEE Robotics and Automation Letters*, vol. 7, no. 2, pp. 2953–2960, 2022.

[36] M. Ramasamy, T. E. Lee, and J. G. Leishman, "Flowfield of a rotating-wing micro air vehicle," *Journal of aircraft*, vol. 44, no. 4, pp. 1236–1244, 2007.

[37] K. Karydis and V. Kumar, "Energetics in robotic flight at small scales," *Interface focus*, vol. 7, no. 1, p. 20160088, 2017.

[38] Q. Quan, *Introduction to multicopter design and control*. Springer, 2017.

[39] R. Prouty, *Helicopter Performance, Stability, and Control*. PWS Engineering, 1986.


**IEEE Robotics and Automation Letters (RA-L) paper, presented at ICRA 2024, Yokohama, Japan. Cite as RA-L paper.**